Research Paper

Protective effects of three herbal extracts on mitochondrial dysfunction in *VPS13C*-knockdown SH-SY5Y cells: implications for Parkinson's disease

Yih-Ru Wu[1,*], Chih-Hsin Lin[1,*], Pei-Syuan Huang[2,*], Chih-Ying Chao[1], Te-Hsien Lin[1], Wan-Ling Chen[1], Chiung-Mei Chen[1], Kuo-Hsuan Chang[1], Ming-Chung Lee[3], I-Cheng Chen[2], Guey-Jen Lee-Chen[2]

[1]Department of Neurology, Chang Gung Memorial Hospital, Chang Gung University College of Medicine, Taoyuan 33378, Taiwan
[2]School of Life Science, National Taiwan Normal University, Taipei 11677, Taiwan
[3]Sun Ten Pharmaceutical Co., Ltd., New Taipei City 23143, Taiwan
*Equal contribution

Correspondence to: I-Cheng Chen, Guey-Jen Lee-Chen; **email:** ichen@ntnu.edu.tw, t43019@ntnu.edu.tw
Keywords: Parkinson's disease, traditional Chinese medicine, VPS13C knockdown, mitochondrial dysfunction, oxidative stress
Received: March 2, 2026 **Accepted:** July 15, 2026 **Published:** August 13, 2026

ABSTRACT

Parkinson's disease (PD) results primarily from the loss of midbrain dopaminergic neurons. Mitochondrial dysfunction may contribute to PD pathogenesis and depletion of vacuolar protein sorting 13 homolog C (VPS13C) leads to mitochondrial dysfunction. Traditional Chinese medicine (TCM) extracts *Uncaria rhynchophylla*, *Gardenia jasminoides*, and *Scutellaria baicalensis* were reported to have anti-PD effects. This study aimed to examine these three extracts for enhancing VPS13C expression and mechanisms of neuroprotection. Using FCCP-mediated oxidative phosphorylation uncoupling or RNA interference-directed *VPS13C* knockdown, reduced cell viability and mitochondrial membrane potential (MMP) accompanied with increased mitochondrial superoxide in human neuroblastoma SH-SY5Y cells were established. Treatment of cells with these extracts increased cell viability, MMP, and reduced the mitochondrial superoxide. In differentiated SH-SY5Y cells with *VPS13C* knockdown, these extracts reduced lactate dehydrogenase release, caspase-3 activity, reactive oxygen species production, and promoted neurite outgrowth. The extracts increased VPS13C, superoxide dismutase (SOD) 1 and 2, nuclear respiratory factor 2 (NRF2), PPARG coactivator 1 alpha (PGC-1α), and B-cell lymphoma 2 (BCL2) expression in these cells, accompanied by increases in MMP, mitochondrial mass, and reduction in mitochondrial superoxide. In conclusion, treatments with these three TCM compounds reduced mitochondrial dysfunction and oxidative stress in *VPS13C*-knockdown cells, making them potential drug candidates for PD.

INTRODUCTION

Parkinson's disease (PD) is a common, genetically complex neurodegenerative disorder that typically affects middle-aged and older adults. PD risk is influenced by a combination of aging, genetic, and environmental factors. PD is characterized by a symptom triad of resting tremors, rigidity, and bradykinesia, which primarily result from dopaminergic neuronal dysfunction and loss in the substantia nigra (SN) and its surrounding regions. PD is pathologically defined by the presence of intracellular neuronal inclusions (i.e., Lewy bodies) in the SN and other brain regions [1].

Various genetic factors contribute to the familial forms of PD [2]. Studies on the pathophysiological roles of relevant genes in patients with PD have uncovered the molecular mechanisms involved in PD pathogenesis. These mechanisms include defects in misfolded protein clearance, excessive oxidative stress, mitochondrial dysfunction, impaired proteasomal degradation and autophagy or mitophagy, and deficits in synaptic vesicle trafficking [3]. Vacuolar protein sorting 13 homolog C (VPS13C; also known as PARK23) belongs to a family of large vacuolar protein sorting 13 proteins crucial for vesicular transport [4]. Biallelic mutations in *VPS13C* are associated with autosomal recessive early-onset parkinsonism and VPS13C deficiency is linked to a loss of the protein [5]. Silencing of *VPS13C* triggers mitochondrial membrane potential (MMP) loss and enhances mitophagy in response to carbonyl cyanide 3-chlorophenyl hydrazone (CCCP)-induced mitochondrial dysfunction [5]. Thus, we selected VPS13C as a therapeutic target in our studies. In mammalian cells, VPS13C localizes to endomembrane system components, such as early endosomes, the Golgi apparatus, the endoplasmic reticulum (ER), and the mitochondrial outer membrane [5]. In addition, VPS13C localizes at contacts between the ER and endosomes or lysosomes, acting as a bridge for lipid transport [6, 7]. Moreover, VPS13C depletion leads to an accumulation of lysosomes with an altered lipid profile [8]. Thus far, 18 VPS13C-related PD cases have been reported; in most of these cases, the clinical response to dopaminergic therapy has appeared to be favorable [9].

Increased oxidative stress significantly mediates PD pathogenesis [10]. Reactive oxygen species (ROS), including the superoxide anion ($O_2^{\bullet-}$), the hydroxyl radical (•OH), and hydrogen peroxide (H_2O_2), are produced from oxygen as byproducts of cellular respiration. ROS are typically maintained at low levels *in vivo*, and a prooxidant–antioxidant imbalance leads to oxidative stress, resulting in neuronal damage and degeneration [11]. In response to oxidative stress, enzymatic antioxidants such as superoxide dismutase (SOD), catalase (CAT), glutathione peroxidase (GPx), and thioredoxin (TRX) aid in maintaining the redox balance by modulating ROS levels [12]. In addition, nuclear respiratory factor 2 (NRF2), a transcription factor, becomes activated to upregulate the expression of PPARG coactivator 1 alpha (PGC-1α) [13]. PGC-1α is a key metabolic regulator that maintains mitochondrial function and neuronal survival [14]. In general, mitochondria represent a main source of intracellular ROS, and excess ROS can result in mitochondrial dysfunction. Tetramethylpyrazine-induced activation of the NRF2/PGC-1α pathway can reduce oxidative stress and enable the maintenance of mitochondrial function in 1-methyl-4-phenyl pyridinium (MPP^+)-induced midbrain neurons and 1-methyl-4-phenyl-1,2,3,6-tetrahydropyridine (MPTP)-induced mice [15]. Therefore, agents targeting NRF2, PGC-1α, or both may have additive benefits in mitigating mitochondrial dysfunction and oxidative stress in PD.

Mitochondria provide cellular energy in the form of ATP through oxidative phosphorylation. Uncoupling of oxidative phosphorylation results in the dissipation of the proton gradient, thereby precluding ATP synthesis. Mitochondrial uncoupling is a key controller of biological processes in physiology and diseases [16]. Increased uncoupling protein 2 expression was detected in affected individuals with the G2019S mutation in the leucine-rich repeat kinase 2 (*LRRK2*) gene [17], the most commonly known genetic cause of late-onset PD involving mitochondrial dysfunction [18]. Carbonyl cyanide 4-(trifluoromethoxy)phenylhydrazone (FCCP), a chemical uncoupler of mitochondrial oxidative phosphorylation [19], is widely validated for studying the effects of acute mitochondrial uncoupling on cellular metabolism and physiology. FCCP has been used to mimic mitochondrial depolarization stress in mouse embryonic fibroblasts with the *LRRK2* R1441G mutation [20]. As mitochondrial dysfunction is biologically relevant to PD, and mitochondrial uncoupler prodrug MP201 protects dopaminergic neurons and improves functional outcome in a mouse model of PD [21], we established screenable phenotypes of FCCP-induced mitochondrial morphology and function in human neuroblastoma SH-SY5Y cells to examine the protective effects of the following three traditional Chinese medicine (TCM) extracts in this study.

Uncaria rhynchophylla (UR; also known as Gou-teng in Chinese) is a commonly used TCM extract to treat various neurological and cerebrovascular diseases [22]. In PD, UR extract exhibits neuroprotective activity against 6-hydroxydopamine (6-OHDA)-induced toxicity through its anti-oxidative and anti-apoptotic properties in PC12 cells *in vitro* and rat PD models *in vivo* [23]. In addition, UR extract can reduce apoptosis and increase MMP against MPP^+/MPTP-induced neurotoxicity in SH-SY5Y cells and PD mouse models [24]. Pharmacokinetic studies have reported the anti-PD activities of the main constituents of UR, including rhynchophylline and isorhynchophylline [25–28].

Gardenia jasminoides (GJ), another herb used in TCM, has various biological properties that positively influence human health. GJ has antioxidant, hypoglycemic, anti-inflammatory, antidepressant, and sleep quality–improving effects [29]. Several bioactive

constituents of GJ, including genipin (aglycone of geniposide) and crocetin (aglycone of crocin), have been isolated and characterized. Geniposide was noted to enhance growth factor signal transduction and reduce apoptosis in an MPTP-induced PD mouse model [30]. Crocin was observed to alleviate nitrosative damage in the striatum of a 6-OHDA-induced PD rat model [31]. Moreover, crocetin was reported to protect dopaminergic neurons in MPTP-induced PD mice and improve mitochondrial function in MPP^+-inflamed BV-2 microglial cells [32]. Finally, GJ extract exerts anti-PD effects via anti-inflammatory and anti-apoptotic mechanisms [33].

Scutellaria baicalensis (SB), commonly referred to as Chinese skullcap, is an herb widely used in TCM to treat respiratory infections, pneumonia, colitis, hepatitis, and allergic diseases [34]. Total flavonoids from SB extract were noted to improve behavior and dopaminergic neuron number in MPTP-induced PD mice [35]. The main bioactive components of SB are flavonoids, including baicalein, wogonin, oroxylin A, baicalin, and wogonoside [34]. Baicalein has been observed to exert neuroprotective effects in different experimental models of PD [36]. Moreover, preclinical PD research has reported a wide range of biological activities of baicalein, including neurotransmitter regulation, enzyme activity modulation, antioxidant and anti-inflammatory activity, protein aggregation inhibition, mitochondrial function improvement, apoptosis inhibition, and MPP^+-induced autophagy prevention [37].

In general, loss of VPS13C function leads to rare recessive forms of PD. Extracts from UR, GJ, and SB may have anti-PD effects. This study investigated the therapeutic effects of these three TCM extracts on *VPS13C*-knockdown SH-SY5Y cells with dopaminergic differentiation induced by the phorbol ester 12-*O*-tetradecanoylphorbol-13-acetate (TPA) [38], with a focus on modulation of oxidative stress and mitochondrial dysfunction. We also used FCCP to induce mitochondrial depolarization, a central mechanism underlying PD pathogenesis, to complement our genetic model and explore the protective effects of the herbal extracts on mitochondrial dysfunction.

RESULTS

TCM extracts

We investigated the effects of TCM extracts UR, GJ, and SB in VPS13C-associated early-onset PD because they have been reported to be beneficial in other PD models. We performed chemical composition analysis on triplicate samples by using liquid chromatography–mass spectrometry (LC-MS) and high-performance liquid chromatography (HPLC). LC-MS analysis (mass-to-charge ratio, *m/z*) revealed the presence of rhynchophylline (*m/z* 386.20; 4.32 ± 0.012 mg/mL) and isorhynchophylline (*m/z* 386.20; 0.63 ± 0.006 mg/mL) in UR extract (200 mg/mL; Figure 1A). HPLC analysis (230 and 450 nm) revealed peaks corresponding to geniposide (20.62 ± 0.045 mg/mL) and crocin (0.36 ± 0.006 mg/mL) in GJ extract (1 g/mL; Figure 1B). When the ultraviolet detection wavelength was set at 280 nm, HPLC analysis revealed that SB extract (1 g/mL) included baicalin, wogonoside, baicalein, wogonin, and oroxylin A at concentrations of 97.19 ± 0.462, 15.90 ± 0.178, 6.60 ± 0.296, 1.78 ± 0.046, and 0.60 ± 0.023 mg/mL, respectively (Figure 1C). We also assessed the cytotoxicity of UR, GJ, and SB extracts (1–1000 μg/mL) in SH-SY5Y cells after 24 h of treatment by performing 3-(4,5-dimethylthiazol-2-yl)-2,5-diphenyl-tetrazolium bromide (MTT) assays. Regardless of concentration, cell viability remained at >90% after treatment with all three herbal extracts (Figure 1D), indicating low cytotoxicity. The studies of chemical composition and cytotoxicity of TCM extracts are crucial for understanding their therapeutic effects and safety.

Uncoupling of oxidative phosphorylation

To induce uncoupling of oxidative phosphorylation, we treated SH-SY5Y cells with FCCP at varied concentrations (20–100 μM), a classical uncoupler of mitochondrial oxidative phosphorylation [19], for 20 h (Figure 2A). The results demonstrated that compared with no FCCP treatment, 40–100 μM FCCP treatment significantly reduced SH-SY5Y cell viability (from 100% to 70%–81%, $p < 0.001$ to $p = 0.001$; Figure 2B). We then used the fluorescent dye 5,5',6,6'-tetrachloro-1,1',3,3'-tetraethyl-benzimidazolylcarbocyanine iodide (JC-1) to measure the cells' MMP. The results demonstrated that 20–100 μM FCCP significantly increased the percentage of low-MMP cells (from 22% to 27%–61%, $p < 0.001$ to $p = 0.013$), accompanied by a decrease in red-to-green fluorescent intensity ratio (from 12.5 to 4.8–9.9, $p < 0.001$; Figure 2C). Furthermore, treatment with 40–100 μM FCCP significantly increased mitochondrial $O_2^{\bullet-}$ production (from 100% to 267%–503%, $p < 0.001$ to $p = 0.006$; Figure 2D). As such, we selected 40 μM FCCP, the lowest concentration significantly affecting cell viability, MMP, and mitochondrial $O_2^{\bullet-}$, to evaluate the protective potential of UR, GJ, and SB extracts against mitochondrial uncoupling.

Effects of TCM extracts in SH-SY5Y cells with mitochondrial uncoupling

SH-SY5Y cells were pretreated with the herbal extracts (10–100 μg/mL) for 4 h, followed by treatment with

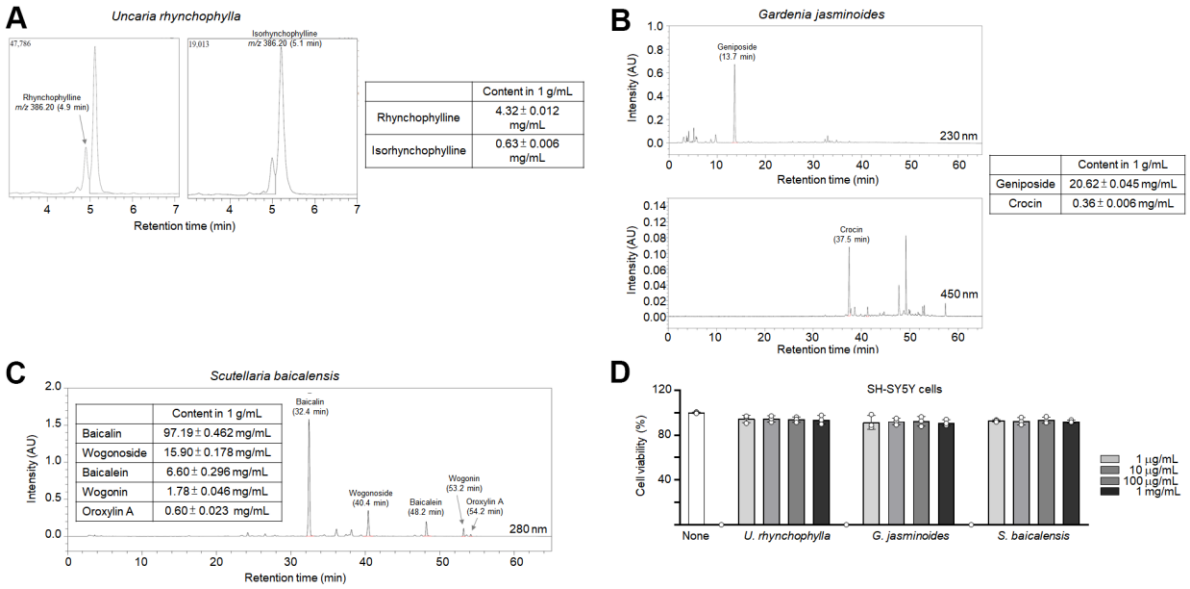

Figure 1. Chemical profiles and cytotoxicity of UR, GJ, and SB extracts. (**A**–**C**) LC-MS and HPLC spectra with peaks of rhynchophylline and isorhynchophylline in UR extract (**A**); peaks of geniposide at 230 nm and crocin at 450 nm in GJ extract (**B**); and peaks of baicalin, wogonoside, baicalein, wogonin, and oroxylin A at 280 nm in SB extract (**C**). Relative amounts of these molecules in 1 g/mL herbal extracts are presented on the right or left side of the spectra (n = 3). (**D**) Results of MTT assay for SH-SY5Y cell viability after treatment with herbal extracts (1 µg/mL to 1 mg/mL) for 24 h (n = 3). The viability of untreated cells (None) was set to 100%.

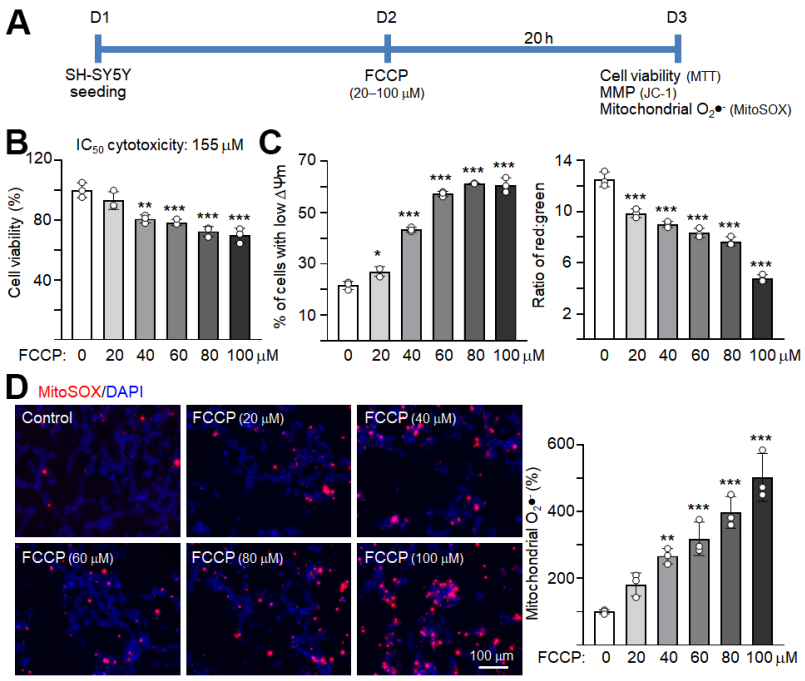

Figure 2. FCCP-uncoupling of mitochondrial oxidative phosphorylation in SH-SY5Y cells. (**A**) Experimental flow chart. SH-SY5Y cells were plated on day 1, treated with FCCP (20-100 µM) on day 2, and analyzed for cell viability (MTT assay), MMP (JC-1 stain), and mitochondrial superoxide (MitoSOX stain) on day 3. (**B**) MTT cell viability assay (n = 3). The viability of untreated cells was set as 100%. (**C**) Flow cytometry analysis of percentage of cells with low MMP (ΔΨm) and red-to-green fluorescent intensity ratio (n = 3). (**D**) High content analysis of mitochondrial superoxide ($O_2^{\bullet-}$) (n = 3). Shown on the left were representative images of analyzed mitochondrial $O_2^{\bullet-}$ using MitoSox staining (red). Cell nuclei counterstained with DAPI (blue). Mitochondrial $O_2^{\bullet-}$ production in FCCP-untreated cells was set as 100%. p-values: FCCP-treated vs. untreated cells (*: $p < 0.05$, **: $p < 0.01$, ***: $p < 0.001$).

40 μM FCCP for 20 h (Figure 3A). As shown in Figure 3B, UR, GJ, and SB extracts at 50–100 μg/mL significantly increased the viability of the FCCP-treated SH-SY5Y cells (from 76% to 96%–102%, $p < 0.001$ to $p = 0.005$). They also significantly reduced the percentage of low-MMP cells (from 40% to 31%–34%, $p < 0.001$ to $p = 0.005$), accompanied by increases in the red-to-green fluorescent intensity ratio (from 8.9 to 11.2–10.6, $p = 0.001$–0.023; Figure 3C), in the FCCP-treated SH-SY5Y cells. Moreover, all three extracts (50–100 μg/mL) significantly reduced mitochondrial $O_2^{\bullet-}$ production in the FCCP-treated SH-SY5Y cells (from 200% to 85%–148%, $p < 0.001$; Figure 3D). We also measured the effects of the herbal extracts on the mitochondrial mass and mitochondrial DNA (mtDNA) content of these cells by using nonyl acridine orange (NAO) staining and multiplex real-time quantitative polymerase chain reaction (qPCR), respectively. At 100 μg/mL, all three herbal extracts significantly increased mitochondrial mass (from 83% to 101%–112%, $p = 0.031$–0.001) and qPCR-based mtDNA content (from 67% to 87%–93%, $p = 0.046$–0.008) in FCCP-treated SH-SY5Y cells (Figure 3E, 3F). The studies of cell viability, MMP, mitochondrial superoxide, mitochondrial mass, and mtDNA content indicated the protective potential of 100 μg/mL UR, GJ, and SB extracts in SH-SY5Y cells with FCCP-induced uncoupling of oxidative phosphorylation.

RNA interference-directed *VPS13C* knockdown

VPS13C silencing in COS-7 and HEK293T cells reduces MMP and exacerbates PTEN induced kinase 1 (PINK1)/parkin RBR E3 ubiquitin protein ligase (PRKN)-dependent mitophagy [5]. The effects of *VPS13C* knockdown in SH-SY5Y cells have not yet been investigated. Thus, to examine the protective potential of the tested UR, GJ, and SB extracts, we established an SH-SY5Y cell–based *in vitro* neuronal PD cell model [39] via *VPS13C* knockdown. In brief, we infected SH-SY5Y cells with lentiviral short hairpin RNA (shRNA) targeting the 3′ end (#151608) or the 5′ end (#151798) of *VPS13C* mRNA or that targeting both (#151608+#151798) for 2 days (Figure 4A). Infection with the combination of 3′ and 5′ end–targeting shRNA effectively reduced *VPS13C* mRNA expression compared with the scrambled control (from 100% to 29%, $p < 0.001$; Figure 4B), accompanied by a decrease in viability (from 100% to 87%, $p < 0.001$), in SH-SY5Y cells (Figure 4C). It also increased the percentage of low-MMP cells (from 35% to 41%, $p = 0.002$), reduced the red-to-green fluorescent intensity ratio (from 5.1 to 4.2, $p = 0.006$; Figure 4D), and promoted mitochondrial $O_2^{\bullet-}$ production (from 100% to 297%, $p < 0.001$; Figure 4E). As a result, we used shRNA targeting both 3′ and 5′ ends of *VPS13C* mRNA to evaluate the protective potential of UR, GJ, and SB extracts in *VPS13C*-knockdown SH-SY5Y cells.

Neuroprotective effects of TCM extracts in *VPS13C*-knockdown SH-SY5Y cells

TPA-treated SH-SY5Y cells are characterized as dopaminergic-like cells. To induce dopaminergic differentiation, we treated SH-SY5Y cells with 120 nM TPA starting on day 2 and continued the treatment for 7 days. The culture medium was replaced with fresh TPA-containing medium every 2–3 days. On day 6, the cells were incubated with lentiviral shRNA (#151608+#151798 or scrambled) overnight to knock down *VPS13C*. To examine the protective effects of the herbal extracts in TPA-differentiated *VPS13C*-knockdown SH-SY5Y cells, we added fresh media containing the herbal extracts (100 μg/mL) to the cells on day 7 and analyzed their effects on day 8 (Figure 5A). The concentration of 100 μg/mL for the herbal extracts in the VPS13C-knockdown experiments was selected based on their protective effects in SH-SY5Y cells subjected to FCCP-induced uncoupling of oxidative phosphorylation (Figure 3). No significant changes in *VPS13C* mRNA expression in scrambled shRNA-infected cells were observed after addition of the herbal extracts (88%–99%, $p > 0.05$). *VPS13C* knockdown significantly reduced *VPS13C* mRNA expression (43%, $p < 0.001$). UR, GJ, or SB extract treatment significantly increased *VPS13C* mRNA expression (70%–85%, $p < 0.001$ to $p = 0.002$; Figure 5B).

Cytotoxicity in *VPS13C*-knockdown cells was evaluated in terms of lactate dehydrogenase (LDH) release and caspase-3 activity. *VPS13C* knockdown significantly increased LDH release (from 12% to 24%, $p < 0.001$) and caspase-3 activity (from 100% to 128%, $p < 0.001$). UR, GJ, or SB extract treatment significantly reduced LDH release (from 24% to 17%–14%, $p = 0.033$–0.003) and caspase-3 activity (from 128% to 78%–98%, $p < 0.001$; Figure 5C). Moreover, the treated cells exhibited decreased cellular ROS production (from 159% to 111%–113%, $p = 0.007$–0.009), indicating the protective role of UR, GJ, and SB extracts in *VPS13C*-knockdown SH-SY5Y cells (Figure 5D).

We next assessed neurite outgrowth of *VPS13C*-knockdown SH-SY5Y cells (Figure 5E) and observed that *VPS13C* knockdown significantly reduced neurite length (from 23.3 μm to 18.4 μm, $p < 0.001$), neurite process number (from 2.38 to 1.84, $p < 0.001$), and neurite branch number (from 0.60 to 0.41, $p = 0.013$). Treatment with the three herbal extracts significantly increased neurite length (from 18.4 μm to 21.2–21.8 μm, $p = 0.012$–0.031), neurite process number (from

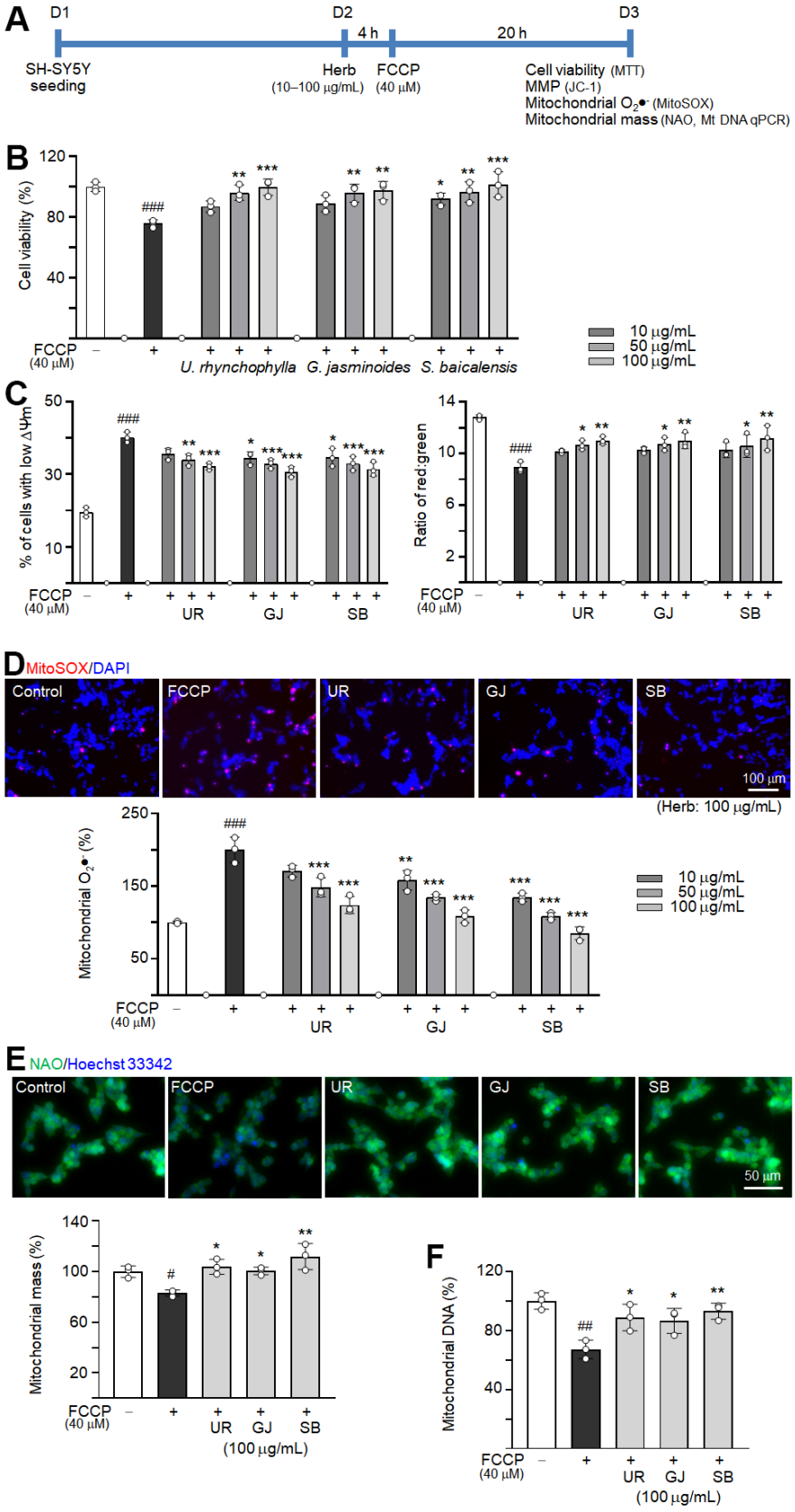

Figure 3. Effects of herbal extracts on SH-SY5Y cells with FCCP-induced uncoupling of mitochondrial oxidative phosphorylation. (**A**) Experimental flow chart. At day 2, SH-SY5Y cells were pretreated with TCM extracts (10-100 μg/mL) for 4 h, and then

treated with FCCP (40 μM) for 20 h. The cells were analyzed for cell viability (MTT assay), MMP (JC-1 stain), mitochondrial superoxide ($O_2^{\bullet-}$; MitoSOX stain), and mitochondrial mass (NAO stain and qPCR of mitochondrial DNA) on day 3. (**B**) MTT cell viability assay (n = 3). The viability of untreated cells was set to 100%. (**C**) Flow cytometry for percentage of cells with low MMP (ΔΨm) and ratio of red-to-green fluorescent intensity (n = 3). (**D**) High content analysis of mitochondrial $O_2^{\bullet-}$ (n = 3). Representative images of mitochondrial $O_2^{\bullet-}$ analysis based on MitoSox staining (red), with cell nuclei counterstained with DAPI (blue), are shown on top. For normalization, mitochondrial $O_2^{\bullet-}$ content in untreated cells was set to 100%. (**E**) High content analysis of mitochondrial mass (n = 3). Representative images of mitochondrial mass based on NAO staining (green), with cell nuclei counterstained with Hoechst 33342 (blue), are shown on top. For normalization, mitochondrial mass in untreated cells was set to 100%. (**F**) qPCR for mtDNA (n = 3). Relative mtDNA content in untreated cells was set to 100%. Data, presented as means ± SDs, were analyzed using one-way ANOVA, followed by Tukey's post hoc test; $^{\#}p < 0.05$, $^{\#\#}p < 0.01$, and $^{\#\#\#}p < 0.001$, compared with cells not treated with FCCP, or $^{*}p < 0.05$, $^{**}p < 0.01$, and $^{***}p < 0.001$, compared with cells not treated with any herbal extract.

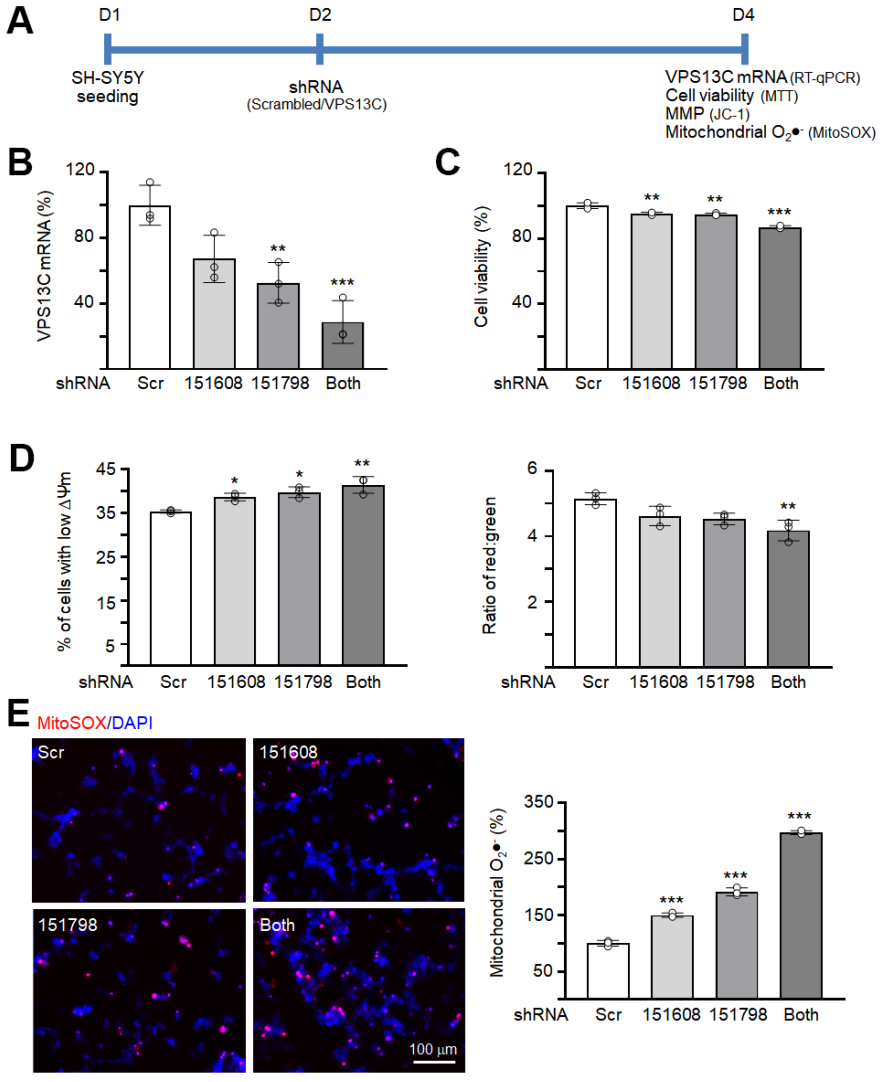

Figure 4. RNA interference-directed *VPS13C* knockdown in SH-SY5Y cells. (**A**) Experimental flow chart. Cells were infected with lentivirus-expressing VPS13C-specific (#151608, #151798, or #151608+#151798) or scrambled shRNA for 2 days. On day 4, cells were collected for *VPS13C* mRNA (reverse transcription qPCR), cell viability (MTT assay), MMP (JC-1 staining), and mitochondrial $O_2^{\bullet-}$ (MitoSOX staining) analyses. (**B**) Reverse transcription qPCR analysis of *VPS13C* mRNA (n = 3). Relative *VPS13C* mRNA content in scrambled shRNA-infected cells was set to 100%. (**C**) MTT assay (n = 3). The viability of scrambled shRNA-infected cells was set to 100%. (**D**) Flow cytometry for percentage of cells with low ΔΨm and red-to-green fluorescent intensity ratio (n = 3). (**E**) High content analysis of mitochondrial $O_2^{\bullet-}$ (n = 3). Representative images of mitochondrial $O_2^{\bullet-}$ analysis based on MitoSox staining (red), with cell nuclei counterstained with DAPI (blue), are shown on top. For normalization, mitochondrial $O_2^{\bullet-}$ content in scrambled shRNA-infected cells was set to 100%. Data, presented as means ± SDs, were analyzed using one-way ANOVA, followed by Tukey's post hoc test; $^{\#}p < 0.05$, $^{\#\#}p < 0.01$, and $^{\#\#\#}p < 0.001$, compared with scrambled shRNA-treated cells.

1.84 to 2.19–2.24, $p = 0.007$–0.017), and neurite branch number (from 0.41 to 0.56–0.58, p = 0.023–0.039). Thus, at 100 μg/mL, UR, GJ, and SB extracts reduced lactate dehydrogenase release, caspase-3 activity, cellular ROS production, while promoting neurite outgrowth in differentiated SH-SY5Y cells with *VPS13C* knockdown.

Improvements in mitochondrial function of *VPS13C*-knockdown SH-SY5Y cells

We subsequently measured expression of VPS13C, SOD (cytoplasmic SOD1 and mitochondrial SOD2 converting superoxide radicals to oxygen and H_2O_2) [40], NRF2 (a key transcription factor in antioxidant defense systems) [41], PGC-1α (a master regulator of mitochondrial biogenesis) [42], and B-cell lymphoma 2 (BCL2; an anti-apoptotic protein) and BCL2-associated X (BAX; a pro-apoptotic protein) [43] in *VPS13C*-knockdown SH-SY5Y cells. As shown in Figure 6A, *VPS13C*-specific shRNA significantly reduced the expression of VPS13C (43%, $p < 0.001$), SOD1 (65%, $p = 0.048$), SOD2 (67%, $p < 0.001$), NRF2 (66%, $p = 0.002$), PGC-1α (67%, $p = 0.003$), and BCL2 (44%, $p < 0.001$) but increased that of BAX (145%, $p < 0.001$). The three herbal extracts significantly reversed the changes in the expression of VPS13C (from 43% to 89%–94%, $p < 0.001$), SOD1 (from 65% to 100%–105%, $p = 0.023$–0.047), SOD2 (from 67% to 96%–101%, $p < 0.001$), NRF2 (from 66% to 92%–98%, $p = 0.003$–0.014), PGC-1α (from 67% to 100%–109%, $p < 0.001$ to $p = 0.003$), BCL2 (from 44% to 97%–107%, $p < 0.001$), and BAX (from 145% to 61%–112%, $p < 0.001$ to $p = 0.003$).

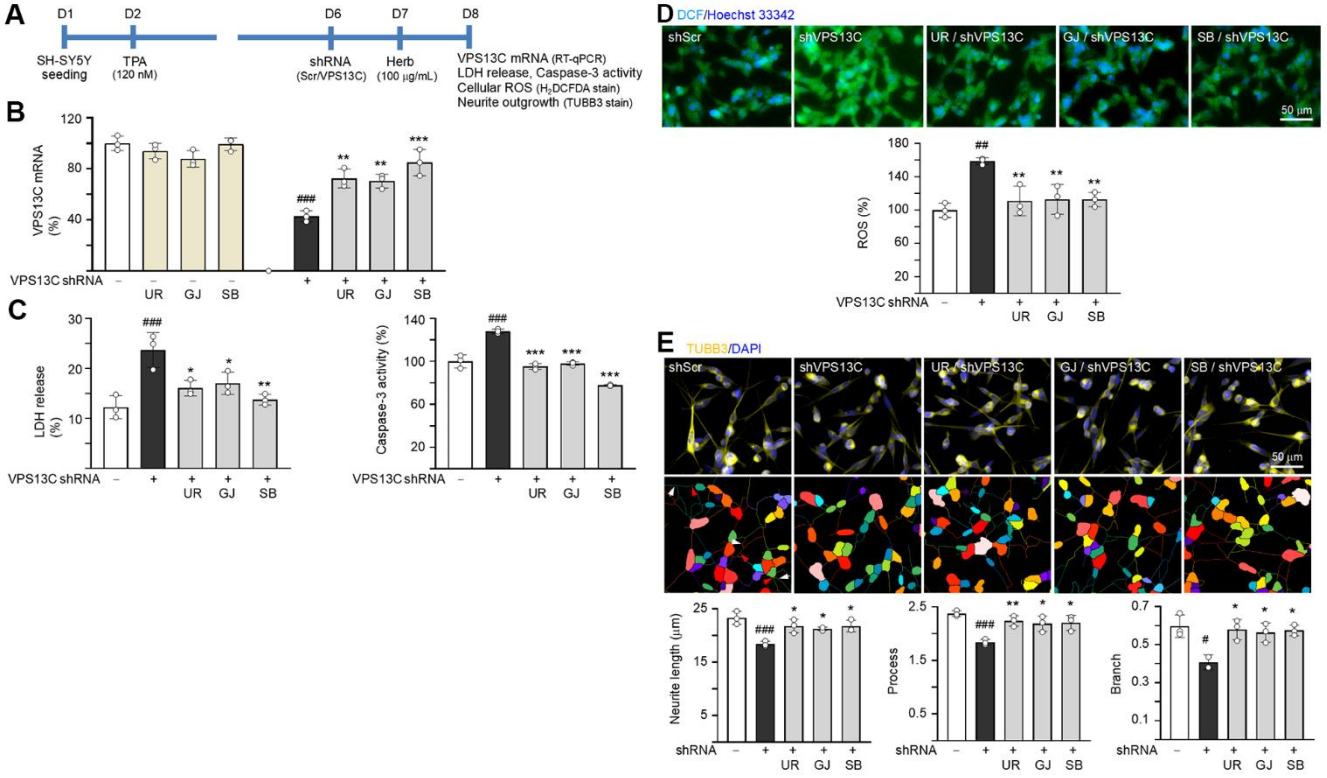

Figure 5. Effects of herbal extracts on TPA-differentiated dopaminergic SH-SY5Y cells with *VPS13C* knockdown. (**A**) Experimental flow chart. On day 2, cells were treated with TPA (120 nM) to induce dopaminergic differentiation for 7 days. Cells were then infected with *VPS13C*-specific shRNA (#151608+#151798) or scrambled shRNA on day 6, followed by a 24-h herbal extract treatment (100 μg/mL) on day 7. (**B**) *VPS13C* mRNA expression (qRT-PCR), (**C**) LDH release and caspase-3 activity, (**D**) cellular ROS (DCF staining; green), and (**E**) neurite length, process, and branch (TUBB3 staining; yellow) were measured on day 8 ($n = 3$). For normalization, relative *VPS13C* mRNA, caspase-3 activity, and cellular ROS levels in scrambled shRNA-infected cells were set to 100%. In (**E**), a multi-colored mask representing a single neuronal cell was applied to the segmented fluorescence images to identify every neuron within the image. This enables the visualization of neuronal identities, providing a quantification of the neurite outgrowth from the cell body. The red and white arrows in the image of scrambled shRNA-treated cells indicate processes and branches, respectively. The total length, process number, and branch number of neurites were calculated. Nuclei were counterstained with DAPI (blue). Data, presented as means ± SDs, were analyzed using one-way ANOVA, followed by Tukey's post hoc test; $^{\#\#\#}p < 0.001$, compared with scrambled shRNA-treated cells, or $^{*}p < 0.05$, $^{**}p < 0.01$, and $^{***}p < 0.001$, compared with cells not treated with any herbal extract.

We then assessed the effects of UR, GJ, and SB extracts on MMP, mitochondrial $O_2^{\bullet-}$, mitochondrial mass, and mtDNA in *VPS13C*-knockdown SH-SY5Y cells. The percentage of cells with low MMP was significantly lower in the cells treated with the herbal extracts (48% vs. 38%–41%, p = 0.004–0.025), and the red-to-green fluorescent intensity ratio was higher in the cells treated with the herbal extracts (3.0 vs. 5.0, p = 0.004; Figure 6B). Moreover, the herbal extracts significantly reduced mitochondrial $O_2^{\bullet-}$ production in the cells (from 249% to 109%–117%, $p < 0.001$; Figure 6C) and significantly increased NAO-assessed mitochondrial mass (from 86% to 101%–105%, p = 0.007–0.027) and mtDNA content (from 78% to 95%, p = 0.024–0.028; Figure 6D, 6E). Thus, UR, GJ, and SB extracts at 100 μg/mL upregulated the expression of VPS13C, SOD1, SOD2, NRF2, PGC-1α, and BCL2. Furthermore, these extracts enhanced mitochondrial function, as evidenced by increased MMP and mitochondrial mass alongside reduced mitochondrial superoxide production in differentiated SH-SY5Y cells with *VPS13C* knockdown.

DISCUSSION

PD has a complex pathogenesis, with mitochondrial dysfunction playing a pivotal role in the development of its sporadic and familial forms [44]. Depletion of VPS13C leads to mitochondrial dysfunction [5]. In *VPS13C*-knockdown SH-SY5Y cells with TPA-induced dopaminergic differentiation, UR, GJ, and SB extracts increased *VPS13C* expression and neurite growth, and reduced LDH release, caspase-3 activity, and cellular ROS production (Figure 5). Furthermore, UR, GJ, and

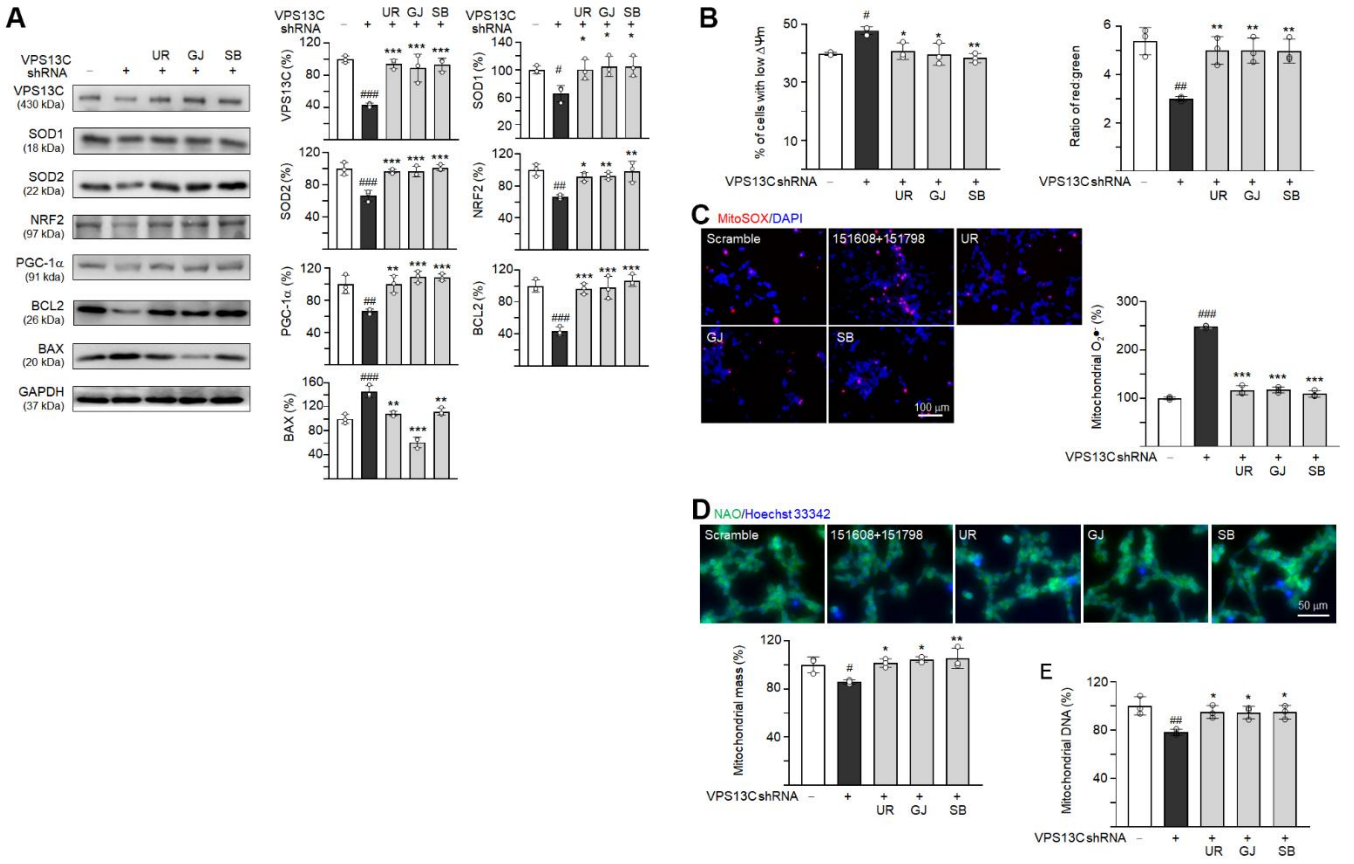

Figure 6. Protective effects of herbal extracts on TPA-differentiated dopaminergic SH-SY5Y cells with *VPS13C* knockdown. In brief, SH-SY5Y cells were differentiated using TPA, infected with lentiviral shRNA, and treated with the herbal extracts. (**A**) Cell protein (VPS13C, SOD1, SOD2, NRF2, PGC-1α, BCL2, and BAX) expression, (**B**) MMP, (**C**) mitochondrial $O_2^{\bullet-}$ content (MitoSOX staining; red), (**D**) mitochondrial mass (NAO staining; green), and (**E**) mtDNA content (qPCR) were measured on day 8 (n = 3). For normalization, the relative levels of VPS13C, SOD1, SOD2, NRF2, PGC-1α, BCL2, BAX, mitochondrial $O_2^{\bullet-}$, mitochondrial mass, and mtDNA in scrambled shRNA-infected cells were set to 100%. Cell nuclei were counterstained with (**C**) DAPI or (**D**) Hoechst 33342 (blue). Data, presented as means ± SDs, were analyzed using one-way ANOVA, followed by Tukey's post hoc test; $^{\#}p < 0.05$, $^{\#\#}p < 0.01$, and $^{\#\#\#}p < 0.001$, compared with scrambled shRNA-treated cells, or $^{*}p < 0.05$, $^{**}p < 0.01$, and $^{***}p < 0.001$, compared with cells not treated with any herbal extract.

SB extracts increased expression of SOD1, SOD2, NRF2, PGC-1α, and BCL2, reduced expression of BAX, increased MMP, reduced mitochondrial $O_2^{\bullet-}$ levels, and increased mitochondrial mass (Figure 6). The study results further support the involvement of VPS13C deficiency in PD pathogenesis and indicate that UR, GJ, and SB extracts may serve as promising therapeutic candidates for PD.

TCM extracts with neuroprotective activity have been used as alternative medicine to treat PD [45]. Oxidative insults and resulting mitochondrial dysfunction may be the leading causes of dopaminergic neuronal degeneration in PD [46]. Therefore, TCM extracts with antioxidant activity may be effective anti-PD agents [47]. In particular, *Ginkgo biloba* extract, with its antioxidant activity, was observed to have potent neuroprotective effects in the MPTP/MPP^+ model of PD [48]. In A53T α-synuclein transgenic mice, *Ginkgo biloba* extract could alleviate oxidative damage and maintain dopamine homeostasis, inhibiting PD development [49]. In the present study, UR, GJ, and SB extracts exerted potent neuroprotective effects by upregulating SOD1 and SOD2 expression in dopaminergic SH-SY5Y cells with *VPS13C* knockdown (Figure 6). Similarly, studies have reported that UR, GJ, and SB extracts increased SOD expression in experimental models of Alzheimer's disease, ischemic brain injury, and skin aging [50–52]. Isorhynchophylline can attenuate MPP^+-induced apoptotic death and oxidative stress in the rat pheochromocytoma cell line PC12 [26]. Geniposide can suppress rotenone-induced neuronal oxidative damage associated with NRF2 signaling in mice [53]. Baicalein can protect against MPP^+-induced oxidative stress in SH-SY5Y cells [54]. Taken together, these results indicate that isorhynchophylline in UR extract, geniposide in GJ extract, and baicalein in SB extract may contribute to the protective effects observed in *VPS13C*-knockdown SH-SY5Y cells. The blood–brain barrier (BBB) is a natural protective barrier that impedes the entry of most chemical drugs and biopharmaceuticals into the brain. Among the major compounds identified in UR, GJ, and SB extracts, isorhynchophylline showed high BBB permeability in the MDCK-pHaMDR cell monolayer model [55]. Geniposide can cross the BBB, show brain-targeted distribution, and exhibit a defined pharmacokinetic profile in brain tissues [56]. Baicalein has been detected in rat brain tissue after oral administration of *Scutellariae Radix* (the dried root of SB) extract using a validated solid-phase extraction–liquid chromatography–tandem mass spectrometry (SPE-LC/MS/MS) method. This finding supports its brain exposure and suggests potential BBB permeability [57]. As such, UR, GJ, and SB extract–induced enhancement of superoxide dismutation (via SOD1/2 upregulation) may be an effective therapeutic approach for mitigating PD progression, in which oxidative stress plays a critical role [58].

Under oxidative stress, cells activate NRF2 signaling to maintain redox homeostasis [59]. In the absence of oxidative stress, NRF2 is constitutively ubiquitinated and degraded via the Kelch-like ECH-associated protein 1 (KEAP1)-mediated proteasomal pathway [60]. In the presence of oxidative stress, NRF2 activation occurs via KEAP1 dissociation, enabling modulation of mitochondrial function [61]. In addition to inducing the expression of multiple genes encoding antioxidant enzymes, experimental evidence has confirmed that NRF2 influences PGC-1α expression, promoting mitochondrial biogenesis [62]. Shende'an tablet, containing the TCM Zhengan Xifeng Decoction, can activate the PGC-1α/NRF2 pathway to protect dopaminergic PC12 cells against 6-OHDA lesions and alleviate motor symptoms in mice subjected to MPTP lesions [63]. In the present study, UR, GJ, and SB extracts increased NRF2 and PGC-1α expression in dopaminergic SH-SY5Y cells with *VPS13C* knockdown (Figure 6), further indicating that UR, GJ, and SB extracts may be promising therapeutic candidates for PD treatment. As ML385, a specific NRF2 inhibitor, was reported to block the anti-PD effects of neuroprotective formononetin [64], future NRF2/PGC-1α pathway inhibition experiments employing ML385 are warranted to confirm the anti-PD effects of UR, GJ, and SB extracts through the NRF2 signaling pathway.

Currently, no disease-modifying treatment is available for PD. Because human dopaminergic neurons are difficult to obtain and maintain as primary cells, SH-SY5Y cells have been widely used to study the molecular and cellular mechanisms underlying PD [65]. SH-SY5Y cell line, a subline of SK-N-SH neuroblastoma, can be induced to differentiate into a more mature neuron-like phenotype through exposure to retinoic acid (RA) [66]. RA treatment can promote SH-SY5Y cell survival [67, 68], and RA-differentiated cells are less vulnerable to 6-OHDA, MPTP, or MPP^+ (a MPTP metabolite) [69, 70]. However, their inadequate responses to chemical insults limit the suitability of SH-SY5Y cells as a neurotoxin-induced PD model. Nevertheless, co-administration of the phorbol ester TPA and RA in SH-SY5Y cells can induce a cholinergic neuron phenotype that is mature and dopaminergic and has high tyrosine hydroxylase (TH), dopamine receptor, and dopamine transporter expression [71]. In addition, simultaneous TPA exposure and serum depletion can enable differentiation of SH-SY5Y cells into dopaminergic neuronal-like cells, suitable to assess lipopolysaccharide-induced neuroinflammatory

responses [72]. Moreover, TPA-treated α-synuclein-expressing dopaminergic-like SH-SY5Y cells demonstrate increased TH expression [73]. Therefore, in the current study, to study the therapeutic effects of the three herbal extracts, we induced dopaminergic differentiation of *VPS13C*-knockdown SH-SY5Y cells by using TPA.

Several limitations of the present study should be acknowledged. Immortalized cell lines lack the complex three-dimensional microenvironment, glial–neuronal interactions, and systemic pharmacokinetic factors present in the human brain. While such models are useful for disease modeling, drug screening, and mechanistic studies, the findings cannot be directly extrapolated to clinical efficacy. In addition, although no cytotoxicity was observed in SH-SY5Y cells, the possibility of adverse effects on other brain cell types cannot be excluded. As *in vitro* cell studies do not provide sufficient biological complexity, future investigations employing primary neuronal cultures, human iPSC-derived dopaminergic neurons, *in vivo* animal models, or multi-model validation approaches should be employed to improve the translational relevance of the findings.

CONCLUSIONS

Mitochondrial dysfunction is strongly associated with PD pathogenesis. Here, we explored the protective effects of three TCM extracts on TPA-differentiated dopaminergic SH-SY5Y cells with *VPS13C* knockdown. UR, GJ, and SB extracts reduced LDH release, caspase-3 activity, and cellular ROS production and promoted neurite growth. Moreover, these herbal extracts increased VPS13C, SOD1, SOD2, NRF2, PGC-1α, and BCL2 expression and reduced BAX expression. These changes were accompanied by increases in MMP and mitochondrial mass and a reduction in mitochondrial $O_2^{\bullet-}$ levels. In general, these findings suggest the therapeutic potential of UR, GJ, and SB extracts in modulating mitochondrial dysfunction associated with PD.

MATERIALS AND METHODS

Herbal extracts

UR, GJ, and SB extracts were provided by Sun Ten Pharmaceutical (New Taipei City, Taiwan). To obtain the extracts, 100 g of each dried herb was immersed in 1,500 mL of water, boiled for 30 min, sieved using a 100-mesh sieve, and concentrated to 100 mL. The obtained herbal extracts were filtered through a 200-mesh sieve, dried through speed vacuum concentration, and stored at −20° C until use. LC-MS analysis of UR extract (200 mg/mL) was performed using a Shimadzu LCMS-2020 system (Shimadzu, Kyoto, Japan), equipped with an SPD-M20A photodiode array detector and an LCMS-2020 mass detector (Herbiotek, New Taipei City, Taiwan). UR extract was subjected to HPLC on a Shim-pack XR-ODS II column (100 × 2.0 mm, 2.2 μm) and eluted with a mixture of 0.1% HCOOH in water (A) and 0.1% HCOOH in methanol solution (B). The linear gradient elution program for A:B (v/v) was set as follows: 75:25 (initial), 35:65 (10 min), 35:65 (12 min), 75:25 (13 min), and 75:25 (18 min); the flow rate was 0.4 mL/min, and the column was maintained at 40° C. Rhynchophylline and isorhynchophylline were used as reference compounds for UR extract [21]. GJ and SB extracts (1 g/mL) were subjected to HPLC on a Waters 600 HPLC system (Waters, Milford, MA, USA), equipped with a Waters 2996 photodiode array detector (Herbiotek) and a Cosmosil 5C18-MS-II column (250 × 4.6 mm, 5 μm). The extracts were eluted with a mixture of 10% H_3PO_4 (A), CH_3CN (B), and water (C). The linear gradient elution program for A:B:C (v/v/v) was set as follows: 90:10:0 (initial), 75:25:0 (30 min), 65:35:0 (40 min), 0:75:25 (55 min), 0:10:90 (60 min), 90:10:0 (65 min); the flow rate was 1 mL/min, and the column was maintained at 35° C. Geniposide and crocin were used as reference compounds for GJ extract [74]. Baicalin, wogonoside, baicalein, wogonin, and oroxylin A were used as reference compounds for SB extract [75, 76]. Absorbance was monitored at 230 nm (geniposide), 450 nm (crocin), and 280 nm (baicalin, wogonoside, baicalein, wogonin, and oroxylin A); the scan range for the photodiode array was set to 190–600 nm. For all HPLC experiments, reference compound concentrations were determined using standard curves, and quantifications were performed in three replicates.

SH-SY5Y cell culture

SH-SY5Y cells (CRL-2266; ATCC, USA), widely used for their undifferentiated or differentiated neuron-like properties in neuroscience research [77], were maintained in Dulbecco's modified Eagle medium/F-12 supplemented with 10% fetal bovine serum (Invitrogen, Carlsbad, CA, USA) at 37° C under 95% humidity and 5% CO_2.

Cytotoxicity assay

MTT, a yellow tetrazolium salt commonly used as an indicator of cell viability, and FCCP, a proton ionophore as an oxidative phosphorylation uncoupler, were purchased from Sigma-Aldrich (St. Louis, MO, USA). SH-SY5Y cells (2×10^4 per well in a 96-well plate) were treated with the herbal extracts (1–1,000 μg/mL) or FCCP (0–100 μM) for 20 h. The absorbance of the purple-colored formazan product was recorded at

570 nm using a Multiskan GO microplate reader (Thermo Fisher Scientific, Waltham, MA, USA).

MMP assay

To examine MMP alterations in our cells, we used JC-1. This fluorescent dye forms aggregates emitting red fluorescence within the mitochondria in healthy cells. JC-1 remains as monomers emitting green fluorescence in cells with MMP loss. In brief, 0–100 μM FCCP-treated cells (1.2×10^5 per well in a 24-well plate) were incubated with JC-1 (5 μM; Invitrogen) for 30 min. The stained cells were rinsed with phosphate-buffered saline (PBS), resuspended in Hanks' balanced salt solution (#14025; Thermo Fisher Scientific), and analyzed using a flow cytometer (FACS Calibur; Becton Dickinson, San Diego, CA, USA) at an excitation wavelength of 488 nm and emission wavelengths of 530 (green) and 585 (red) nm. In total, 10^4 cells were analyzed in each sample.

Mitochondrial $O_2^{\bullet-}$ assay

We used a fluorogenic dye targeted to mitochondria in live cells to examine the levels of mitochondrial $O_2^{\bullet-}$, a redox signaling agent generated via the mitochondrial respiratory chain. In brief, 0–100 μM FCCP-treated cells (2×10^4 per well in a 96-well plate) were incubated with MitoSox Red (5 μM; Invitrogen) and Hoechst 33342 (0.1 μg/mL; Thermo Fisher Scientific) for 30 min. The cells were then imaged using an ImageXpress Micro Confocal (Molecular Devices, Sunnyvale, CA, USA) at 488-nm excitation and 510-nm emission wavelengths to measure $O_2^{\bullet-}$ levels and 377-nm excitation and 447-nm emission wavelengths to detect nuclei. For each sample, approximately 3,000 cells were analyzed in each of three independent experiments.

Herbal extract treatment and mitochondrial uncoupling

To examine the protective effects of the herbal extracts on FCCP-uncoupled oxidative phosphorylation, SH-SY5Y cells were treated with UR, GJ, or SB extract (10–100 μg/mL) for 4 h, followed by treatment with 40 μM FCCP for 20 h. Cell viability, mitochondrial $O_2^{\bullet-}$ (2×10^4 cells per well in a 96-well plate), and MMP (1.2×10^5 cells per well in a 24-well plate) were analyzed. Mitochondrial mass (1.2×10^5 cells per well in a 24-well plate) and mtDNA (2.5×10^5 cells per well in a 24-well plate) were also assessed, as described in subsequent subsections.

Mitochondrial mass and mtDNA assays

Mitochondrial mass was assayed using the fluorescent probe 10-N NAO (Thermo Fisher Scientific). NAO binds to the mitochondrial marker lipid cardiolipin, and this binding is independent of the mitochondria's energization state in a membrane potential-independent manner [78]. In brief, cells were incubated with 10 μM NAO and 0.1 μg/mL Hoechst 33342 for 15 min. Next, the cells were imaged using an ImageXpress Micro Confocal at 475-nm excitation and 536-nm emission wavelengths to measure mitochondrial mass and 377-nm excitation and 447-nm emission wavelengths to detect nuclei. For each sample, approximately 3,000 cells were analyzed in each of three independent experiments.

mtDNA content was assessed using multiplex qPCR, as described elsewhere [79]. DNA was extracted from SH-SY5Y cells by using standard protocols. Each sample was run in triplicate on a 96-well plate in a 10-μL reaction containing 40 ng of DNA. The cycle threshold (Ct) value was determined from the amplification curve for mitochondrially encoded NADH dehydrogenase 1 (*ND1*; ID: Hs02596873_s1; NC_012920.ND1.0: exon boundary: 1, context sequence: TCTACATCACCGCC CCGACCTTAGC, amplicon length: 143 bp) and nuclear ribonuclease P RNA component H1 (*RPPH1*; ID: Hs03297761_s1; NR_002312.1: exon boundary: 1, context sequence: TGGAACAGACTCACGGCCAGC GAAG, amplicon length: 68 bp) on a StepOnePlus™ Real-time PCR system (Applied Biosystems, Foster City, CA, USA). Fold changes in mtDNA copy number were calculated relative to the control group using the $2^{-\Delta\Delta Ct}$ method, where $\Delta\Delta Ct = \Delta Ct$ (target sample) − ΔCt (control sample) and $\Delta Ct = Ct$ (*ND1*) − Ct (*RPPH1*).

RNA interference

Lentiviral shRNA targeting *VPS13C* (TRCN0000151608 and TRCN0000151798) and a negative scrambled control (TRC2.Void) were obtained from the National RNAi Core Facility, IMB/GRC, Academia Sinica (Taipei, Taiwan). On day 1, we plated SH-SY5Y cells at 6×10^5 per well in a 6-well plate for *VPS13C* mRNA analysis, 1.2×10^5 per well in a 24-well plate for MMP analysis, and 2×10^4 cells per well in a 96-well plate for cell viability and mitochondrial $O_2^{\bullet-}$ analyses. On day 2, the cells were treated with lentivirus (multiplicity of infection = 3) and polybrene (8 μg/mL; Sigma-Aldrich) and left to incubate overnight. On day 3, the medium containing lentivirus and polybrene was removed. On day 4, the cells were harvested for further analyses.

On day 1, cells were also seeded at 3×10^5 per well in a 6-well plate for *VPS13C* mRNA, LDH, caspase-3, and protein analyses; 1.2×10^5 per well in a 12-well plate for mtDNA analysis; 6×10^4 per well in a 24-well plate

for cellular ROS, neurite outgrowth, MMP, and mitochondrial mass analyses; or 10^4 per well in a 96-well plate for mitochondrial $O_2^{\bullet-}$ analysis. TPA (120 nM; Enzo Life Sciences, Farmingdale, NY, USA) was added to SH-SY5Y cells on day 2 to promote dopaminergic differentiation [37]. The cells were then cultured in the presence of polybrene (8 μg/mL) during lentivirus transduction (multiplicity of infection = 3) on day 6. Next, the transduction medium was replaced with a fresh complete medium to remove lentivirus and polybrene. The cells were treated with the herbal extracts (100 μg/mL) on day 7 and harvested for further analyses on day 8. The following hairpin sequences of targeting and scrambled shRNA were used:

(1) TRCN0000151608 (targeting at the 3′ end of *VPS13C*: 12,962–12,982 of NM_020821): 5′-CCGGGCAGTAACTAATGCCCTAAATctcgagATTTAGGGCATTAGTTACTGCTTTTTTG-3′
(2) TRCN0000151798 (targeting at the 5′ end of *VPS13C*: 1,633–1,653 of NM_020821): 5′-CCGGCCTAACTTTACCTAAGCAGTActcgagTACTGCTTAGGTAAAGTTAGGTTTTTTG-3′
(3) TRC2.Void (scrambled negative control): 5′-CCGGAGTTCAGTTACGATATCATGTctcgagACATTCGCGAGTAACTGAACTTTTTT-3′

Reverse transcription qPCR

RNA was extracted from SH-SY5Y cells by using TRIzol reagent (Invitrogen), and residual DNA was removed using DNase I (Stratagene, La Jolla, CA, USA). cDNA was synthesized using SuperScript™ III reverse transcriptase (Invitrogen). Expression of *VPS13C* (ID: Hs00419559_m1; NM_001018088.2: exon boundary: 55–56, context sequence: AGGCTTGATGTAAAGAAGAACCCAG, amplicon length: 96 bp) and housekeeping hypoxanthine phosphoribosyl transferase 1 (*HPRT1*; endogenous control; ID: 4326321E; NM_000194.2: exon boundary: 6–7, context sequence: TGGTCAAGGTCGCAAGCTTGCTGGT, amplicon length: 100 bp) was determined using a StepOnePlus™ Real-time PCR system (Applied Biosystems). Fold changes were calculated relative to the control group using the $2^{-\Delta\Delta Ct}$ method, where ΔΔCt = ΔCt (target sample) − ΔCt (control sample) and ΔCt = Ct (*VPS13C*) − Ct (*HPRT1*).

LDH release and caspase-3 activity assays

We used an LDH cytotoxicity assay kit (Cayman Chemical, Ann Arbor, MI, USA) to measure the levels of cytosolic LDH released from TPA-differentiated SH-SY5Y cells into culture medium. The cell culture medium and reaction mixture were mixed and incubated for 30 min. Next, absorbance was measured at 490 nm by using a microplate reader (Multiskan GO; Thermo Fisher Scientific). Absorbance of cells treated with 10% Triton X-100 was set to 100%.

To assay caspase-3 activity, cells (6×10^5 per well in a 6-well plate) were collected in cold PBS and lysed via six freeze–thaw cycles. In 10 μg of supernatant, caspase-3 activity was assessed by measuring the fluorescent release of 7-amino-4-methylcoumarin (AMC) from a substrate acetyl-Asp-Glu-Val-Asp-AMC (Ac-DEVD-AMC; Sigma-Aldrich) using an excitation wavelength of 360 nm and an emission wavelength of 460 nm (FLx800; Bio-Tek).

Total ROS assay

An ROS-reactive fluorogenic probe was used to measure the ROS formed in SH-SY5Y cells. In brief, the cells were incubated with cell-permeant 2′,7′-dichlorodihydrofluorescein diacetate (25 μM; Invitrogen) and Hoechst 33342 (0.1 μg/mL; Sigma-Aldrich) at 37° C for 30 min. Cells were imaged using an ImageXpress Micro Confocal at 475-nm excitation and 536-nm emission to measure cellular $O_2^{\bullet-}$ levels and 377-nm excitation and 447-nm emission wavelengths to detect nuclei. For each sample, approximately 3,000 cells were analyzed in each of three independent experiments.

Neurite outgrowth assessment

SH-SY5Y cells were fixed in 0.4% paraformaldehyde for 16–24 h, permeabilized with 0.1% Triton X-100 for 10 min, blocked in 3% bovine serum albumin for 3 h, and stained with an antibody raised against neuronal class III β-tubulin (TUBB3; 1:1000; #802001; BioLegend, San Diego, CA, USA) at 4° C overnight. Next, the cells were incubated with donkey anti-rabbit Alexa Fluor 555 secondary antibody (1:1000; Invitrogen #A-31572) at room temperature for 3 h, followed by nuclear staining with 4′,6-diamidino-2-phenylindole (DAPI; 0.1 μg/mL; Sigma-Aldrich) for 30 min. The cells were imaged at 531-nm excitation and 593-nm emission wavelengths to measure neurite outgrowths and 377-nm excitation and 447-nm emission wavelengths to detect nuclei. We measured total neurite length and the number of processes (projections from the neuronal cell body) and branches (projections from neural processes) by using the MetaXpress neurite outgrowth application module (Molecular Devices). For each sample, approximately 3,000 cells were analyzed in each of three independent experiments.

Immunoblot analysis

Proteins were extracted from SH-SY5Y cells by using a lysis buffer containing 150 mM sodium chloride, 50 mM

Tris-HCl, pH 8.0, 1 mM EDTA, pH 8.0, 1 mM EGTA, pH 8.0, 0.1% SDS, 0.5% sodium deoxycholate, 1% Triton X-100, and protease inhibitor cocktail (Sigma-Aldrich). Next, protein concentrations were quantified using a protein assay kit from Bio-Rad (Hercules, CA, USA), and 10-μg proteins were separated using sodium dodecyl sulfate–polyacrylamide (8%–12%) gel electrophoresis and transferred to polyvinylidene difluoride (PVDF) membranes (Sigma-Aldrich) in a Mini Trans-Blot cell (Bio-Rad). The blotted PVDF membranes were probed with primary antibodies against VPS13C (1:1000; #28676-1-AP; Proteintech, Rosemont, IL, USA), SOD1 (1:500; #sc-17767; Santa Cruz Biotechnology, Santa Cruz, CA, USA), SOD2 (1:5000; #13141; Cell Signaling, Danvers, MA, USA), NRF2 (1:1000; #12721; Cell Signaling), PGC-1α (1:1000; #GTX37356; GeneTex, Irvine, CA, USA), BCL2 (1:1000; #IR94-392; iReal Biotechnology, Hsinchu City, Taiwan), BAX (1:1000; #2772; Cell Signaling), or glyceraldehyde-3-phosphate dehydrogenase (GAPDH; 1:1000; #30000002; MDBio, Taipei, Taiwan) overnight at 4° C. The immune complexes that formed were detected using a 1:5000 dilution of goat anti-rabbit (#GTX213110-01; GeneTex) or goat anti-mouse (#GTX213111-01; GeneTex) immunoglobulin G conjugated with horseradish peroxidase and chemiluminescent substrate (Millipore, Temecula, CA, USA).

Statistical analysis

To ensure the reproducibility and reliability of the results, all assays were performed in triplicate (three technical replicates) in three independent experiments (three biological replicates), and the results are presented as means ± standard deviations (SDs). Statistical comparisons among groups were performed using one-way analysis of variance (ANOVA) followed by Tukey's post hoc test. A p-value of <0.05 was considered to indicate statistical significance.

ACKNOWLEDGMENTS

We thank the Instrumentation Center of National Taiwan Normal University for their support and assistance in this work.

AUTHOR CONTRIBUTIONS

YRW and GJLC conceived the manuscript and designed the experiments. CHL and PSH conducted the experiments. CHL, PSH, and GJLC analyzed data. YRW, ICC, and GJLC wrote the manuscript. CYC, THL, WLC, and MCL provided reagents and materials. CMC and KHC critically revised the manuscript. YRW, ICC, and GJLC revised the manuscript. All authors have read and approved the final manuscript.

CONFLICTS OF INTEREST

The authors declare that they have no conflicts of interest.

FUNDING

This work was supported by the Ministry of Science and Technology (MOST 109-2314-B-182A-077-MY3, 109-2811-B-182A-514, 110-2811-B-182A-515, and 111-2811-B-182A-008).

REFERENCES

1. Gibb WR, Lees AJ. The significance of the Lewy body in the diagnosis of idiopathic Parkinson's disease. Neuropathol Appl Neurobiol. 1989; 15:27–44. https://doi.org/10.1111/j.1365-2990.1989.tb01147.x PMID:2542825

2. Westenberger A, Brüggemann N, Klein C. Genetics of Parkinson's Disease: From Causes to Treatment. Cold Spring Harb Perspect Med. 2025; 15:a041774. https://doi.org/10.1101/cshperspect.a041774 PMID:39134389

3. Xiao B, Zhou Z, Chao Y, Tan EK. Pathogenesis of Parkinson's Disease. Neurol Clin. 2025; 43:185–207. https://doi.org/10.1016/j.ncl.2024.12.003 PMID:40185518

4. Velayos-Baeza A, Vettori A, Copley RR, Dobson-Stone C, Monaco AP. Analysis of the human VPS13 gene family. Genomics. 2004; 84:536–49. https://doi.org/10.1016/j.ygeno.2004.04.012 PMID:15498460

5. Lesage S, Drouet V, Majounie E, Deramecourt V, Jacoupy M, Nicolas A, Cormier-Dequaire F, Hassoun SM, Pujol C, Ciura S, Erpapazoglou Z, Usenko T, Maurage CA, et al., and French Parkinson's Disease Genetics Study (PDG), and International Parkinson's Disease Genomics Consortium (IPDGC). Loss of VPS13C Function in Autosomal-Recessive Parkinsonism Causes Mitochondrial Dysfunction and Increases PINK1/Parkin-Dependent Mitophagy. Am J Hum Genet. 2016; 98:500–13. https://doi.org/10.1016/j.ajhg.2016.01.014 PMID:26942284

6. Cai S, Wu Y, Guillén-Samander A, Hancock-Cerutti W, Liu J, De Camilli P. *In situ* architecture of the lipid transport protein VPS13C at ER-lysosome membrane contacts. Proc Natl Acad Sci USA. 2022; 119:e2203769119. https://doi.org/10.1073/pnas.2203769119 PMID:35858323

7. Kumar N, Leonzino M, Hancock-Cerutti W, Horenkamp FA, Li P, Lees JA, Wheeler H, Reinisch KM, De Camilli P.

VPS13A and VPS13C are lipid transport proteins differentially localized at ER contact sites. J Cell Biol. 2018; 217:3625–39. https://doi.org/10.1083/jcb.201807019 PMID:30093493

8. Hancock-Cerutti W, Wu Z, Xu P, Yadavalli N, Leonzino M, Tharkeshwar AK, Ferguson SM, Shadel GS, De Camilli P. ER-lysosome lipid transfer protein VPS13C/PARK23 prevents aberrant mtDNA-dependent STING signaling. J Cell Biol. 2022; 221:e202106046. https://doi.org/10.1083/jcb.202106046 PMID:35657605

9. Monfrini E, Spagnolo F, Canesi M, Seresini A, Rini A, Passarella B, Percetti M, Seia M, Goldwurm S, Cereda V, Comi GP, Pezzoli G, Di Fonzo A. VPS13C-associated Parkinson's disease: Two novel cases and review of the literature. Parkinsonism Relat Disord. 2022; 94:37–9. https://doi.org/10.1016/j.parkreldis.2021.11.031 PMID:34875562

10. Prasuhn J, Davis RL, Kumar KR. Targeting Mitochondrial Impairment in Parkinson's Disease: Challenges and Opportunities. Front Cell Dev Biol. 2021; 8:615461. https://doi.org/10.3389/fcell.2020.615461 PMID:33469539

11. Rahal A, Kumar A, Singh V, Yadav B, Tiwari R, Chakraborty S, Dhama K. Oxidative stress, prooxidants, and antioxidants: the interplay. Biomed Res Int. 2014; 2014:761264. https://doi.org/10.1155/2014/761264 PMID:24587990

12. He L, He T, Farrar S, Ji L, Liu T, Ma X. Antioxidants Maintain Cellular Redox Homeostasis by Elimination of Reactive Oxygen Species. Cell Physiol Biochem. 2017; 44:532–53. https://doi.org/10.1159/000485089 PMID:29145191

13. Athale J, Ulrich A, MacGarvey NC, Bartz RR, Welty-Wolf KE, Suliman HB, Piantadosi CA. Nrf2 promotes alveolar mitochondrial biogenesis and resolution of lung injury in Staphylococcus aureus pneumonia in mice. Free Radic Biol Med. 2012; 53:1584–94. https://doi.org/10.1016/j.freeradbiomed.2012.08.009 PMID:22940620

14. Panes JD, Wendt A, Ramirez-Molina O, Castro PA, Fuentealba J. Deciphering the role of PGC-1α in neurological disorders: from mitochondrial dysfunction to synaptic failure. Neural Regen Res. 2022; 17:237–45. https://doi.org/10.4103/1673-5374.317957 PMID:34269182

15. Guo B, Zheng C, Cao J, Luo F, Li H, Hu S, Mingyuan Lee S, Yang X, Zhang G, Zhang Z, Sun Y, Wang Y. Tetramethylpyrazine nitrone exerts neuroprotection via activation of PGC-1α/Nrf2 pathway in Parkinson's disease models. J Adv Res. 2024; 64:195–211. https://doi.org/10.1016/j.jare.2023.11.021 PMID:37989471

16. Demine S, Renard P, Arnould T. Mitochondrial Uncoupling: A Key Controller of Biological Processes in Physiology and Diseases. Cells. 2019; 8:795. https://doi.org/10.3390/cells8080795 PMID:31366145

17. Grünewald A, Arns B, Meier B, Brockmann K, Tadic V, Klein C. Does uncoupling protein 2 expression qualify as marker of disease status in LRRK2-associated Parkinson's disease? Antioxid Redox Signal. 2014; 20:1955–60. https://doi.org/10.1089/ars.2013.5737 PMID:24251413

18. Buck SA, Sanders LH. LRRK2-mediated mitochondrial dysfunction in Parkinson's disease. Biochem J. 2025; 482:721–39. https://doi.org/10.1042/BCJ20253062 PMID:40440058

19. Heytler PG, Prichard WW. A new class of uncoupling agents--carbonyl cyanide phenylhydrazones. Biochem Biophys Res Commun. 1962; 7:272–5. https://doi.org/10.1016/0006-291x(62)90189-4 PMID:13907155

20. Chang EE, Liu H, Choi ZY, Malki Y, Zhang SX, Pang SY, Kung MH, Ramsden DB, Ho SL, Ho PW. Loss of mitochondrial Ca^{2+} response and CaMKII/ERK activation by $LRRK2^{R1441G}$ mutation correlate with impaired depolarization-induced mitophagy. Cell Commun Signal. 2024; 22:485. https://doi.org/10.1186/s12964-024-01844-y PMID:39390438

21. Kishimoto Y, Johnson J, Fang W, Halpern J, Marosi K, Liu D, Geisler JG, Mattson MP. A mitochondrial uncoupler prodrug protects dopaminergic neurons and improves functional outcome in a mouse model of Parkinson's disease. Neurobiol Aging. 2020; 85:123–30. https://doi.org/10.1016/j.neurobiolaging.2019.09.011 PMID:31718928

22. Yang W, Ip SP, Liu L, Xian YF, Lin ZX. Uncaria rhynchophylla and its Major Constituents on Central Nervous System: A Review on Their Pharmacological Actions. Curr Vasc Pharmacol. 2020; 18:346–57. https://doi.org/10.2174/1570161117666190704092841 PMID:31272356

23. Shim JS, Kim HG, Ju MS, Choi JG, Jeong SY, Oh MS. Effects of the hook of Uncaria rhynchophylla on neurotoxicity in the 6-hydroxydopamine model of Parkinson's disease. J Ethnopharmacol. 2009; 126:361–5. https://doi.org/10.1016/j.jep.2009.08.023 PMID:19703534

24. Lan YL, Zhou JJ, Liu J, Huo XK, Wang YL, Liang JH, Zhao JC, Sun CP, Yu ZL, Fang LL, Tian XG, Feng L, Ning J, et al.

Uncaria rhynchophylla Ameliorates Parkinson's Disease by Inhibiting HSP90 Expression: Insights from Quantitative Proteomics. Cell Physiol Biochem. 2018; 47:1453–64. https://doi.org/10.1159/000490837 PMID:29940559

25. Hu S, Mak S, Zuo X, Li H, Wang Y, Han Y. Neuroprotection Against MPP^+-Induced Cytotoxicity Through the Activation of PI3-K/Akt/GSK3β/MEF2D Signaling Pathway by Rhynchophylline, the Major Tetracyclic Oxindole Alkaloid Isolated From Uncaria rhynchophylla. Front Pharmacol. 2018; 9:768. https://doi.org/10.3389/fphar.2018.00768 PMID:30072894

26. Li XM, Zhang XJ, Dong MX. Isorhynchophylline Attenuates MPP^+-Induced Apoptosis Through Endoplasmic Reticulum Stress- and Mitochondria-Dependent Pathways in PC12 Cells: Involvement of Antioxidant Activity. Neuromolecular Med. 2017; 19:480–92. https://doi.org/10.1007/s12017-017-8462-x PMID:28822073

27. Lu JH, Tan JQ, Durairajan SS, Liu LF, Zhang ZH, Ma L, Shen HM, Chan HY, Li M. Isorhynchophylline, a natural alkaloid, promotes the degradation of alpha-synuclein in neuronal cells via inducing autophagy. Autophagy. 2012; 8:98–108. https://doi.org/10.4161/auto.8.1.18313 PMID:22113202

28. Zheng M, Chen M, Wang W, Zhou M, Liu C, Fan Y, Shi D. Protection by rhynchophylline against MPTP/MPP^+-induced neurotoxicity via regulating PI3K/Akt pathway. J Ethnopharmacol. 2021; 268:113568. https://doi.org/10.1016/j.jep.2020.113568 PMID:33188898

29. Xiao W, Li S, Wang S, Ho CT. Chemistry and bioactivity of Gardenia jasminoides. J Food Drug Anal. 2017; 25:43–61. https://doi.org/10.1016/j.jfda.2016.11.005 PMID:28911543

30. Chen Y, Zhang Y, Li L, Hölscher C. Neuroprotective effects of geniposide in the MPTP mouse model of Parkinson's disease. Eur J Pharmacol. 2015; 768:21–7. https://doi.org/10.1016/j.ejphar.2015.09.029 PMID:26409043

31. Hosseini M, Rajaei Z, Alaei H, Tajadini M. The Effects of Crocin on 6-OHDA-Induced Oxidative/Nitrosative Damage and Motor Behaviour in Hemiparkinsonian Rats. Malays J Med Sci. 2016; 23:35–43. https://doi.org/10.21315/mjms2016.23.6.4 PMID:28090177

32. Dong N, Dong Z, Chen Y, Gu X. Crocetin Alleviates Inflammation in MPTP-Induced Parkinson's Disease Models through Improving Mitochondrial Functions. Parkinsons Dis. 2020; 2020:9864370. https://doi.org/10.1155/2020/9864370 PMID:33101635

33. Hou Z, Sun L, Jiang Z, Zeng T, Wu P, Huang J, Liu H, Xiao P. Neuropharmacological insights into Gardenia jasminoides Ellis: Harnessing therapeutic potential for central nervous system disorders. Phytomedicine. 2024; 125:155374. https://doi.org/10.1016/j.phymed.2024.155374 PMID:38301302

34. Liao H, Ye J, Gao L, Liu Y. The main bioactive compounds of Scutellaria baicalensis Georgi. for alleviation of inflammatory cytokines: A comprehensive review. Biomed Pharmacother. 2021; 133:110917. https://doi.org/10.1016/j.biopha.2020.110917 PMID:33217688

35. Li XL, Xu XF, Bu QX, Jin WR, Sun QR, Feng DP, Zhang QJ, Wang LX. Effect of total flavonoids from Scutellaria baicalensis on dopaminergic neurons in the substantia nigra. Biomed Rep. 2016; 5:213–6. https://doi.org/10.3892/br.2016.713 PMID:27446544

36. Zhu Q, Zhuang X, Lu J. Neuroprotective effects of baicalein in animal models of Parkinson's disease: A systematic review of experimental studies. Phytomedicine. 2019; 55:302–9. https://doi.org/10.1016/j.phymed.2018.09.215 PMID:30385133

37. Wang Y, Wei N, Li X. Preclinical Evidence and Possible Mechanisms of Baicalein for Rats and Mice With Parkinson's Disease: A Systematic Review and Meta-Analysis. Front Aging Neurosci. 2020; 12:277. https://doi.org/10.3389/fnagi.2020.00277 PMID:33101006

38. Påhlman S, Odelstad L, Larsson E, Grotte G, Nilsson K. Phenotypic changes of human neuroblastoma cells in culture induced by 12-O-tetradecanoyl-phorbol-13-acetate. Int J Cancer. 1981; 28:583–9. https://doi.org/10.1002/ijc.2910280509 PMID:7309295

39. Ioghen OC, Ceafalan LC, Popescu BO. SH-SY5Y Cell Line *In Vitro* Models for Parkinson Disease Research-Old Practice for New Trends. J Integr Neurosci. 2023; 22:20. https://doi.org/10.31083/j.jin2201020 PMID:36722247

40. Zelko IN, Mariani TJ, Folz RJ. Superoxide dismutase multigene family: a comparison of the CuZn-SOD (SOD1), Mn-SOD (SOD2), and EC-SOD (SOD3) gene structures, evolution, and expression. Free Radic Biol Med. 2002; 33:337–49. https://doi.org/10.1016/s0891-5849(02)00905-x PMID:12126755

41. Niture SK, Kaspar JW, Shen J, Jaiswal AK. Nrf2 signaling and cell survival. Toxicol Appl Pharmacol. 2010; 244:37–42. https://doi.org/10.1016/j.taap.2009.06.009 PMID:19538984

42. Jornayvaz FR, Shulman GI. Regulation of mitochondrial biogenesis. Essays Biochem. 2010; 47:69–84. https://doi.org/10.1042/bse0470069 PMID:20533901

43. Harada H, Grant S. Apoptosis regulators. Rev Clin Exp Hematol. 2003; 7:117–38. PMID:14763159

44. Bose A, Beal MF. Mitochondrial dysfunction in Parkinson's disease. J Neurochem. 2016; 139:216–31. https://doi.org/10.1111/jnc.13731 PMID:27546335

45. Chen P, Zhang J, Wang C, Chai YH, Wu AG, Huang NY, Wang L. The pathogenesis and treatment mechanism of Parkinson's disease from the perspective of traditional Chinese medicine. Phytomedicine. 2022; 100:154044. https://doi.org/10.1016/j.phymed.2022.154044 PMID:35338993

46. Guo JD, Zhao X, Li Y, Li GR, Liu XL. Damage to dopaminergic neurons by oxidative stress in Parkinson's disease (Review). Int J Mol Med. 2018; 41:1817–25. https://doi.org/10.3892/ijmm.2018.3406 PMID:29393357

47. Muhammad F, Liu Y, Zhou Y, Yang H, Li H. Antioxidative role of Traditional Chinese Medicine in Parkinson's disease. J Ethnopharmacol. 2022; 285:114821. https://doi.org/10.1016/j.jep.2021.114821 PMID:34838943

48. Rojas P, Montes P, Rojas C, Serrano-García N, Rojas-Castañeda JC. Effect of a phytopharmaceutical medicine, Ginko biloba extract 761, in an animal model of Parkinson's disease: therapeutic perspectives. Nutrition. 2012; 28:1081–8. https://doi.org/10.1016/j.nut.2012.03.007 PMID:22817828

49. Kuang S, Yang L, Rao Z, Zhong Z, Li J, Zhong H, Dai L, Tang X. Effects of Ginkgo Biloba Extract on A53T α-Synuclein Transgenic Mouse Models of Parkinson's Disease. Can J Neurol Sci. 2018; 45:182–7. https://doi.org/10.1017/cjn.2017.268 PMID:29506601

50. Xu QQ, Shaw PC, Hu Z, Yang W, Ip SP, Xian YF, Lin ZX. Comparison of the chemical constituents and anti-Alzheimer's disease effects of Uncaria rhynchophylla and Uncaria tomentosa. Chin Med. 2021; 16:110. https://doi.org/10.1186/s13020-021-00514-2 PMID:34706756

51. Zhang H, Lai Q, Li Y, Liu Y, Yang M. Learning and memory improvement and neuroprotection of Gardenia jasminoides (Fructus gardenia) extract on ischemic brain injury rats. J Ethnopharmacol. 2017; 196:225–35. https://doi.org/10.1016/j.jep.2016.11.042 PMID:27940085

52. Sun G, Dang Y, Lin Y, Zeng W, Wu Z, Zhang X, Dong D, Wu B. Scutellaria baicalensis Georgi regulates REV-ERBα/BMAL1 to protect against skin aging in mice. Front Pharmacol. 2022; 13:991917. https://doi.org/10.3389/fphar.2022.991917 PMID:36249807

53. Zhou Q, Chen B, Xu Y, Wang Y, He Z, Cai X, Qin Y, Ye J, Yang Y, Shen J, Cao P. Geniposide protects against neurotoxicity in mouse models of rotenone-induced Parkinson's disease involving the mTOR and Nrf2 pathways. J Ethnopharmacol. 2024; 318:116914. https://doi.org/10.1016/j.jep.2023.116914 PMID:37451492

54. Song Q, Peng S, Zhu X. Baicalein protects against MPP^+/MPTP-induced neurotoxicity by ameliorating oxidative stress in SH-SY5Y cells and mouse model of Parkinson's disease. Neurotoxicology. 2021; 87:188–94. https://doi.org/10.1016/j.neuro.2021.10.003 PMID:34666128

55. Zhang YN, Yang YF, Xu W, Yang XW. The Blood-Brain Barrier Permeability of Six Indole Alkaloids from Uncariae Ramulus Cum Uncis in the MDCK-pHaMDR Cell Monolayer Model. Molecules. 2017; 22:1944. https://doi.org/10.3390/molecules22111944 PMID:29125571

56. Qu K, Zhao L, Luo X, Zhang C, Hou P, Bi K, Chen X. An LC-MS method for simultaneous determination of five iridoids from Zhi-zi-chi Decoction in rat brain microdialysates and tissue homogenates: towards an in depth study for its antidepressive activity. J Chromatogr B Analyt Technol Biomed Life Sci. 2014; 965:206–15. https://doi.org/10.1016/j.jchromb.2014.03.032 PMID:25049209

57. Fong SY, Wong YC, Zuo Z. Development of a SPE-LC/MS/MS method for simultaneous quantification of baicalein, wogonin, oroxylin A and their glucuronides baicalin, wogonoside and oroxyloside in rats and its application to brain uptake and plasma pharmacokinetic studies. J Pharm Biomed Anal. 2014; 97:9–23. https://doi.org/10.1016/j.jpba.2014.03.033 PMID:24803030

58. Zaman V, Shields DC, Shams R, Drasites KP, Matzelle D, Haque A, Banik NL. Cellular and molecular pathophysiology in the progression of Parkinson's disease. Metab Brain Dis. 2021; 36:815–27. https://doi.org/10.1007/s11011-021-00689-5 PMID:33599945

59. Kasai S, Shimizu S, Tatara Y, Mimura J, Itoh K. Regulation of Nrf2 by Mitochondrial Reactive Oxygen Species in Physiology and Pathology. Biomolecules. 2020; 10:320. https://doi.org/10.3390/biom10020320 PMID:32079324

60. Itoh K, Tong KI, Yamamoto M. Molecular mechanism activating Nrf2-Keap1 pathway in regulation of adaptive response to electrophiles. Free Radic Biol Med. 2004; 36:1208–13. https://doi.org/10.1016/j.freeradbiomed.2004.02.075 PMID:15110385

61. Itoh K, Ye P, Matsumiya T, Tanji K, Ozaki T. Emerging functional cross-talk between the Keap1-Nrf2 system and mitochondria. J Clin Biochem Nutr. 2015; 56:91–7. https://doi.org/10.3164/jcbn.14-134 PMID:25759513

62. Deng X, Lin N, Fu J, Xu L, Luo H, Jin Y, Liu Y, Sun L, Su J. The Nrf2/PGC1 α Pathway Regulates Antioxidant and Proteasomal Activity to Alter Cisplatin Sensitivity in Ovarian Cancer. Oxid Med Cell Longev. 2020; 2020:4830418. https://doi.org/10.1155/2020/4830418 PMID:33294122

63. Sheng X, Yang S, Wen X, Zhang X, Ye Y, Zhao P, Zang L, Peng K, Du E, Li S. Neuroprotective effects of Shende'an tablet in the Parkinson's disease model. Chin Med. 2021; 16:18. https://doi.org/10.1186/s13020-021-00429-y PMID:33549148

64. Wang X, Kang N, Liu Y, Xu G. Formononetin Exerts Neuroprotection in Parkinson's Disease via the Activation of the Nrf2 Signaling Pathway. Molecules. 2024; 29:5364. https://doi.org/10.3390/molecules29225364 PMID:39598753

65. Xicoy H, Wieringa B, Martens GJ. The SH-SY5Y cell line in Parkinson's disease research: a systematic review. Mol Neurodegener. 2017; 12:10. https://doi.org/10.1186/s13024-017-0149-0 PMID:28118852

66. Kovalevich J, Langford D. Considerations for the use of SH-SY5Y neuroblastoma cells in neurobiology. Methods Mol Biol. 2013; 1078:9–21. https://doi.org/10.1007/978-1-62703-640-5_2 PMID:23975817

67. Itano Y, Ito A, Uehara T, Nomura Y. Regulation of Bcl-2 protein expression in human neuroblastoma SH-SY5Y cells: positive and negative effects of protein kinases C and A, respectively. J Neurochem. 1996; 67:131–7. https://doi.org/10.1046/j.1471-4159.1996.67010131.x PMID:8666983

68. López-Carballo G, Moreno L, Masiá S, Pérez P, Barettino D. Activation of the phosphatidylinositol 3-kinase/Akt signaling pathway by retinoic acid is required for neural differentiation of SH-SY5Y human neuroblastoma cells. J Biol Chem. 2002; 277:25297–304. https://doi.org/10.1074/jbc.M201869200 PMID:12000752

69. Cheung YT, Lau WK, Yu MS, Lai CS, Yeung SC, So KF, Chang RC. Effects of all-trans-retinoic acid on human SH-SY5Y neuroblastoma as *in vitro* model in neurotoxicity research. Neurotoxicology. 2009; 30:127–35. https://doi.org/10.1016/j.neuro.2008.11.001 PMID:19056420

70. Khwanraj K, Phruksaniyom C, Madlah S, Dharmasaroja P. Differential Expression of Tyrosine Hydroxylase Protein and Apoptosis-Related Genes in Differentiated and Undifferentiated SH-SY5Y Neuroblastoma Cells Treated with MPP(.). Neurol Res Int. 2015; 2015:734703. https://doi.org/10.1155/2015/734703 PMID:26634154

71. Presgraves SP, Ahmed T, Borwege S, Joyce JN. Terminally differentiated SH-SY5Y cells provide a model system for studying neuroprotective effects of dopamine agonists. Neurotox Res. 2004; 5:579–98. https://doi.org/10.1007/BF03033178 PMID:15111235

72. Niaz A, Karunia J, Mandwie M, Keay KA, Musumeci G, Al-Badri G, Castorina A. Robust Dopaminergic Differentiation and Enhanced LPS-Induced Neuroinflammatory Response in Serum-Deprived Human SH-SY5Y Cells: Implication for Parkinson's Disease. J Mol Neurosci. 2021; 71:565–82. https://doi.org/10.1007/s12031-020-01678-6 PMID:32789724

73. Chen CM, Yen CY, Chen WL, Lin CH, Wu YR, Chang KH, Lee-Chen GJ. Pathomechanism Characterization and Potential Therapeutics Identification for Parkinson's Disease Targeting Neuroinflammation. Int J Mol Sci. 2021; 22:1062. https://doi.org/10.3390/ijms22031062 PMID:33494411

74. Gao L, Zhu BY. The Accumulation of Crocin and Geniposide and Transcripts of Phytoene Synthase during Maturation of Gardenia jasminoides Fruit. Evid Based Complement Alternat Med. 2013; 2013:686351. https://doi.org/10.1155/2013/686351 PMID:23634173

75. Du Z, Wang K, Tao Y, Chen L, Qiu F. Purification of baicalin and wogonoside from Scutellaria baicalensis extracts by macroporous resin adsorption chromatography. J Chromatogr B Analyt Technol Biomed Life Sci. 2012; 908:143–9. https://doi.org/10.1016/j.jchromb.2012.09.024 PMID:23040984

76. Li HB, Chen F. Isolation and purification of baicalein, wogonin and oroxylin A from the medicinal plant Scutellaria baicalensis by high-speed counter-current chromatography. J Chromatogr A. 2005; 1074:107–10. https://doi.org/10.1016/j.chroma.2005.03.088 PMID:15941045

77. Lopez-Suarez L, Awabdh SA, Coumoul X, Chauvet C. The SH-SY5Y human neuroblastoma cell line, a relevant *in vitro* cell model for investigating neurotoxicology in human: Focus on organic pollutants. Neurotoxicology. 2022; 92:131–55. https://doi.org/10.1016/j.neuro.2022.07.008 PMID:35914637

78. Maftah A, Petit JM, Ratinaud MH, Julien R. 10-N nonyl-acridine orange: a fluorescent probe which stains mitochondria independently of their energetic state. Biochem Biophys Res Commun. 1989; 164:185–90. https://doi.org/10.1016/0006-291x(89)91700-2 PMID:2478126

79. Ashar FN, Moes A, Moore AZ, Grove ML, Chaves PH, Coresh J, Newman AB, Matteini AM, Bandeen-Roche K, Boerwinkle E, Walston JD, Arking DE. Association of mitochondrial DNA levels with frailty and all-cause mortality. J Mol Med (Berl). 2015; 93:177–86. https://doi.org/10.1007/s00109-014-1233-3 PMID:25471480